

Charge radii of exotic neon and magnesium isotopes

S. J. Novario ^{1,2}, G. Hagen ^{2,1}, G. R. Jansen,^{3,2} and T. Papenbrock ^{1,2}

¹*Department of Physics and Astronomy, University of Tennessee, Knoxville, Tennessee 37996, USA*

²*Physics Division, Oak Ridge National Laboratory, Oak Ridge, Tennessee 37831, USA*

³*National Center for Computational Sciences, Oak Ridge National Laboratory, Oak Ridge, Tennessee 37831, USA*



(Received 22 July 2020; accepted 30 October 2020; published 20 November 2020)

We compute the charge radii and ground-state energies of even-mass neon and magnesium isotopes from neutron number $N = 8$ to the dripline. Our calculations are based on nucleon-nucleon and three-nucleon potentials from chiral effective field theory that include Δ isobars. These potentials yield an accurate saturation point and symmetry energy of nuclear matter. We use the coupled-cluster method and start from an axially symmetric reference state. Binding energies and two-neutron separation energies largely agree with data, and the dripline in neon is accurate. The computed charge radii are accurate for many isotopes where data exist. Finer details, such as isotope shifts, however, are not accurately reproduced. These chiral potentials indicate a subshell closure at $N = 14$ for the radii (but not for two-neutron separation energies) and a decrease in charge radii at $N = 8$ (observed in neon and predicted for magnesium). They yield a continued increase of charge radii as neutrons are added beyond $N = 14$ yet underestimate the large increase at $N = 20$ in magnesium.

DOI: [10.1103/PhysRevC.102.051303](https://doi.org/10.1103/PhysRevC.102.051303)

Introduction. The radii of atomic nuclei carry information about their structure as isotopic trends reflect changes in nuclear deformation, shell structure, superconductivity (pairing), and weak binding. The difference between the radii of the neutron and proton distributions of an atomic nucleus also impact the structure of neutron stars. Matter radii are usually extracted from reactions with strongly interacting probes, which requires a model-dependent analysis [1,2]. In contrast, electric charge radii (and more recently also weak charge radii) can be determined using the precisely known electroweak interaction [3,4]. Precision measurements of nuclear charge radii have contributed much to our understanding of stable nuclei and rare isotopes, and they continue to challenge nuclear structure theory [5–8].

In the past two decades we have seen a lot of progress in *ab initio* computations of nuclei, i.e., calculations that employ only controlled approximations and are based on Hamiltonians that link the nuclear many-body problem to the nucleon-nucleon and few-nucleon systems. Virtually exact methods [9–12] scale exponentially with increasing mass number and depend on the exponential increase of available computational cycles for progress. A game changer has been combining ideas and soft interactions from effective field theory (EFT) [13–18] and the renormalization group [19–21] with approximate (but systematically improvable) approaches that scale polynomially with mass number. Examples of such methods are coupled-cluster (CC) theory [22–24], in-medium similarity renormalization group [25,26], nuclear lattice EFT [27,28], symmetry-adapted shell model [29], and self-consistent Green’s function approaches [30,31].

Nuclei as heavy as ^{100}Sn have now been computed within this *ab initio* approach [32,33], and the first *ab initio* survey

of nuclei up to mass 50 or so has appeared [34]. Computing nuclei within this framework is much more costly than using, e.g., nuclear density-functional theory [35–37]. However, the ever-increasing availability of computational cycles makes these computations both feasible and increasingly affordable.

In this Rapid Communication, we compute the charge radii of neutron-rich isotopes of neon and magnesium. These nuclei are at the center of the island of inversion [39,40] and at the focus of current experimental interests. Charge radii are known for $^{17-28}\text{Ne}$ [41–43] and $^{21-32}\text{Mg}$ [38] leaving much to explore. The experimental situation for magnesium isotopes and our theoretical calculations (described in detail below) are shown in Fig. 1. Of particular interest is the impact (or lack thereof) of the “magic” neutron numbers $N = 8, 14,$ and 20 on charge radii, the onset of deformation past $N = 20$, and the rotational structure of neutron-rich isotopes as the dripline is approached [44,45].

Among the many available interactions from chiral EFT [15–17,46–50], the next-to-next-to leading order potentials NNLO_{sat} [18] and $\Delta\text{NNLO}_{\text{GO}}$ [51–53] stand out through their quality in describing nuclear radii. These interactions contain pion physics, three-nucleon forces, and—in the case of $\Delta\text{NNLO}_{\text{GO}}$ —effects of the Δ isobars. Both interactions have been constrained by data on the nucleon-nucleon interaction, and nuclei with mass numbers $A = 3, 4$. Although NNLO_{sat} also was constrained by binding energies and radii of nuclei as heavy as oxygen, $\Delta\text{NNLO}_{\text{GO}}$ was constrained by the binding energy, density and symmetry energy of nuclear matter at its saturation point. These potentials use the leading-order three-body forces from chiral EFT [54]. In this Rapid Communication we will employ two $\Delta\text{NNLO}_{\text{GO}}$ inter-

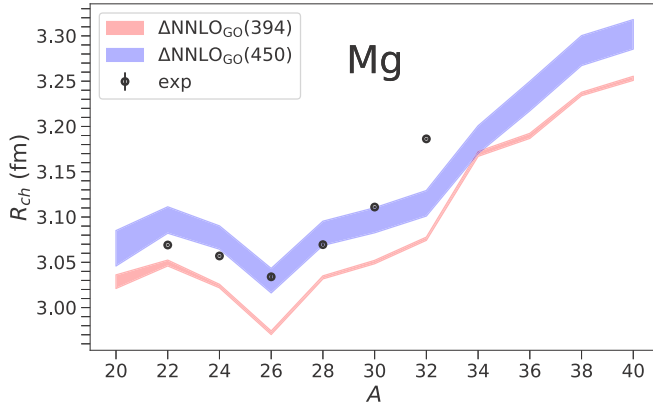


FIG. 1. Charge radii for magnesium isotopes with even mass numbers computed with the potentials $\Delta\text{NNLO}_{\text{GO}}(394)$ (red) and $\Delta\text{NNLO}_{\text{GO}}(450)$ (blue) compared to data (black points) [38]. The model spaces consist of 13 oscillator shells with oscillator frequencies $\hbar\omega = 12$ and 16 MeV as indicated by the bands.

actions which differ by their respective momentum cutoffs of 394 and 450 $\text{MeV}c^{-1}$. The interaction $\Delta\text{NNLO}_{\text{GO}}(394)$ is as soft as the 1.8/2.0(EM) interaction of Ref. [17], while $\Delta\text{NNLO}_{\text{GO}}(450)$ is as hard as NNLO_{sat} [18]. Nuclei as heavy as ^{100}Sn have been converged with the former [32,33,55], whereas the latter has been used for somewhat lighter nuclei [4,50,56–58].

Theoretical approach. Our coupled-cluster calculations start from an axially deformed product state built from natural orbitals. To construct the natural orbitals we start from a spherical harmonic-oscillator basis and perform a Hartree-Fock calculation that keeps axial, parity, and time-reversal symmetries. To obtain the axially symmetric deformed reference state we fill the partially occupied neutron and proton shells at the Fermi surface from low to high values of $|j_z|$. This creates a Hartree-Fock reference state with prolate deformation, and we checked that this state gives a lower energy than starting from an oblate reference (i.e., filling the high values of $|j_z|$ first). The self-consistent solution of the Hartree-Fock equations then yields a prolate deformed product state with the lowest energy. Following Ref. [59] we then compute the density matrix in second-order perturbation theory and diagonalize it to obtain the natural orbitals. As shown in Fig. 2 and discussed below, natural orbitals improve the convergence of the ground-state energies with respect to the number of three-particle–three-hole ($3p$ - $3h$) amplitudes in the coupled-cluster wave function.

The natural orbital basis is spanned by up to 13 spherical harmonic-oscillator shells. We present results for two different oscillator frequencies ($\hbar\omega = 12$ and 16 MeV) to gauge the model-space dependence. These values are close to the simple estimate $\omega \approx \frac{\hbar\Lambda}{2mR}$ that relates the optimal oscillator frequency to the cutoff Λ of the interaction and the radius R of the nucleus [60]. The three-nucleon interaction had the additional energy cut of $E_{3\text{max}} = N_1 + N_2 + N_3 \leq 16\hbar\omega$, where $N_i = 2n_i + l_i$ are single-particle energies. This cut is

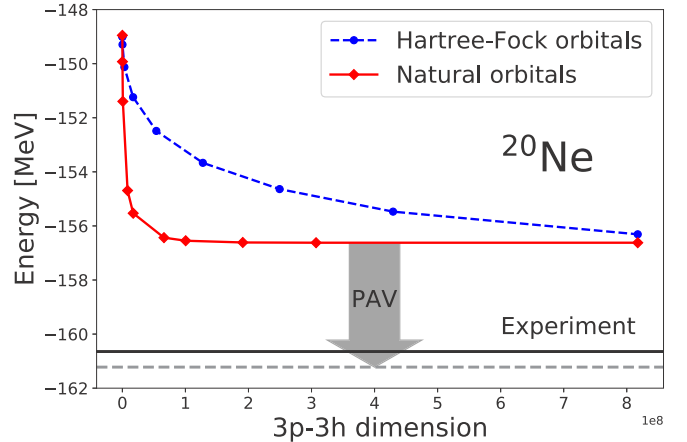


FIG. 2. Ground-state energy of ^{20}Ne with respect to the number of included $3p$ - $3h$ amplitudes, computed from the Hartree-Fock basis (blue circles connected by a dashed line), and natural orbitals (red diamonds connected by a full line). For the Hartree-Fock basis we limited the number of $3p$ - $3h$ excitations by the energy cut $\tilde{E}_{pqr} = \tilde{\epsilon}_p + \tilde{\epsilon}_q + \tilde{\epsilon}_r < \tilde{E}_{3\text{max}}$, where $\tilde{\epsilon}_p = |N_p - N_F|$ is the energy difference between the single-particle energies and the Fermi surface N_F . The cut in the natural orbital basis is described in the main text. We used the $\Delta\text{NNLO}_{\text{GO}}(394)$ potential and a model space of 11 major spherical oscillator shells with the frequency $\hbar\omega = 16$ MeV. The black solid line is the experimental value, whereas the gray dashed line includes the energy gain from projection after variation of the Hartree-Fock result.

sufficient to converge the energies and radii reported in this Rapid Communication.

The breaking of rotational symmetry by the reference state is consistent with the emergent symmetry breaking and captures the correct structure of the nontrivial vacuum [61]. However, our approach lacks possible triaxial deformation and symmetry restoration for which several proposals exist [62–65]. Overcoming these limitations is, thus, possible but comes at a significant increase in computational cost: The loss of symmetries (either by permitting triaxiality or by rotating the Hamiltonian during projection) significantly increases the number of nonzero Hamiltonian matrix elements and coupled-cluster amplitudes. To estimate the impact of symmetry restoration we performed projection after variation of the deformed Hartree-Fock states for all nuclei considered in this Rapid Communication and found an energy gain from 3 to 6 MeV. This provides us with an upper limit on the energy that can be gained through symmetry restoration as we would expect that correlations beyond the mean-field partially restore broken symmetries. We note that triaxial deformations in the ground state are not expected to be significant for the nuclei we study in this Rapid Communication [66]. We finally note that the axially symmetric coupled-cluster computations are an order of magnitude more expensive than those that keep rotational invariance. Fortunately, the availability of leadership-class computing facilities and the use of graphics processor units (GPUs) now make such computations possible.

Our calculations start from the “bare” Hamiltonian,

$$H = T_{\text{kin}} - T_{\text{CoM}} + V_{NN} + V_{NNN} \quad (1)$$

based on the $\Delta\text{NNLO}_{\text{GO}}$ nucleon-nucleon and three-nucleon potentials V_{NN} and V_{NNN} , respectively. Here, T_{kin} denotes the kinetic energy, and we subtract the kinetic energy of the center-of-mass (CoM) T_{CoM} to remove the center of mass from the Hamiltonian. We express this Hamiltonian in terms of operators \hat{a}_p^\dagger and \hat{a}_q that create and annihilate a nucleon with quantum numbers p and q , respectively, in the natural orbital basis. The Hamiltonian H_N is normal ordered with respect to the reference state, and we only retain up to normal-ordered two-body forces; we have $H_N = F_N + V_N$ where the Fock term F_N denotes the normal-ordered one-body part and V_N the normal-ordered two-body terms [67]. We note that the normal-ordered two-body approximation breaks rotational invariance. In the case of particle-number-breaking methods a solution has been proposed in Ref. [68].

The coupled-cluster method [22–24,69–73] generates a similarity-transformed Hamiltonian,

$$\bar{H}_N \equiv e^{-\hat{T}} H_N e^{\hat{T}}, \quad (2)$$

using the cluster-excitation operator,

$$\begin{aligned} \hat{T} &= \hat{T}_1 + \hat{T}_2 + \hat{T}_3 \dots \\ &= \sum_{ia} t_i^a \hat{a}_a^\dagger \hat{a}_i + \frac{1}{4} \sum_{ijab} t_{ij}^{ab} \hat{a}_a^\dagger \hat{a}_b^\dagger \hat{a}_j \hat{a}_i \\ &\quad + \frac{1}{36} \sum_{ijkabc} t_{ijk}^{abc} \hat{a}_a^\dagger \hat{a}_b^\dagger \hat{a}_c^\dagger \hat{a}_k \hat{a}_j \hat{a}_i + \dots \end{aligned} \quad (3)$$

The operator \hat{T}_n creates n -particle– n -hole excitations of the reference state $|\psi\rangle \equiv \prod_{i=1}^A \hat{a}_i^\dagger |0\rangle$. Here and in what follows, labels i, j, k refer to single-particle states occupied in the reference state, whereas a, b, c are for unoccupied states.

We truncate the expansion (3) at the $3p$ - $3h$ level and include leading-order triples using the CC singles, doubles, and linearized triples (CCSDT-1) approximation [74,75]. In this approximation $e^{\hat{T}} \approx e^{\hat{T}_1 + \hat{T}_2} + \hat{T}_3$, and the amplitudes t_i^a , t_{ij}^{ab} , and t_{ijk}^{abc} fulfill

$$\begin{aligned} \langle \psi_i^a | \bar{H}_N + H_N \hat{T}_3 | \psi \rangle &= 0, \\ \langle \psi_{ij}^{ab} | \bar{H}_N + H_N \hat{T}_3 | \psi \rangle &= 0, \\ \langle \psi_{ijk}^{abc} | (F_N \hat{T}_3 + V_N \hat{T}_2)_{\text{con}} | \psi \rangle &= 0. \end{aligned} \quad (4)$$

In the first two lines $\hat{T} = \hat{T}_1 + \hat{T}_2$ enters the similarity transformation, which gives the commonly used CCSD approximation when $\hat{T}_3 = 0$. In the last line only the connected terms enter. The correlation energy is then $E_0 = \langle \psi | \bar{H}_N | \psi \rangle$.

The CCSD approximation costs $\mathcal{O}(u^4)$ compute cycles for each iteration with $o = A$ and u being the number of occupied and unoccupied states, respectively. The cost of CCSDT-1 is $\mathcal{O}(u^4)$ and, thus, an order of magnitude more expensive.

Both CCSD and CCSDT-1 are too expensive without further optimizations. To overcome this challenge we first take advantage of the block-diagonal structure of the Hamiltonian imposed by axial symmetry, isospin, and parity and only store

and process matrix elements that obey these symmetries. Second, we impose a truncation on the allowed number of $3p$ - $3h$ amplitudes by a cut on the product occupation probabilities n_p for three particles above the Fermi surface and for three holes below the Fermi surface, i.e., we require $n_a n_b n_c \leq \varepsilon$ and $(1 - n_i)(1 - n_j)(1 - n_k) \leq \varepsilon$. This cut favors configurations with large occupation probabilities near the Fermi surface and—as shown in Fig. 2—requires only a manageable number of $3p$ - $3h$ amplitudes to be included. Third, we exploit the internal structure of the three-body symmetry blocks, which can be expressed as the tensor product of two- and one-body symmetry blocks, to formulate the equations as a series of matrix multiplications. This allows us to efficiently utilize the supercomputer Summit at the Oak Ridge Leadership Computing Facility, whose computational power mainly comes from GPUs.

For the computation of observables other than the energy (the radius in our case), we also need to solve the left eigenvalue problem as the similarity transformed Hamiltonian is non-Hermitian. This is performed using the equation-of-motion coupled-cluster method (EOM), see Refs. [24,72,75,76] for details. In this Rapid Communication we limit the computations of radii to the EOM-CCSD approximation level. For ^{32}Mg the inclusion of (computationally expensive) triples via the EOM-CCSDT-1 approximation [75] increases the radius by less than 1%, consistent with the findings of Refs. [57,77].

In EOM-CCSDT-1 the left ground-state eigenvalue problem is

$$\langle \psi | (1 + \hat{\Lambda}) \bar{H}_N = E_0 \langle \psi | (1 + \hat{\Lambda}). \quad (5)$$

Here $\hat{\Lambda}$ is a deexcitation operator with amplitudes Λ_a^i , Λ_{ab}^{ij} , and Λ_{abc}^{ijk} . We need to solve for

$$\begin{aligned} \hat{\Lambda} &= \hat{\Lambda}_1 + \hat{\Lambda}_2 + \hat{\Lambda}_3 \\ &= \sum_{ia} \Lambda_a^i \hat{a}_i^\dagger \hat{a}_a + \frac{1}{4} \sum_{ijab} \Lambda_{ab}^{ij} \hat{a}_i^\dagger \hat{a}_j^\dagger \hat{a}_b \hat{a}_a \\ &\quad + \frac{1}{36} \sum_{ijkabc} \Lambda_{abc}^{ijk} \hat{a}_i^\dagger \hat{a}_j^\dagger \hat{a}_k^\dagger \hat{a}_c \hat{a}_b \hat{a}_a. \end{aligned} \quad (6)$$

Given \bar{H}_N , Eq. (5) is an eigenvalue problem, and we are only interested in its ground-state solution $E = E_0$. In the EOM-CCSDT-1 approximation, the triples deexcitation part $\hat{\Lambda}_3$ only contributes to the doubles deexcitation part of the matrix-vector product via $\langle \psi | \hat{\Lambda}_3 V_N | \psi_{ab}^{ij} \rangle$, while the triples deexcitation part of the matrix-vector product is $\langle \psi | (\hat{\Lambda}_1 + \hat{\Lambda}_2) V_N + (\hat{\Lambda}_2 + \hat{\Lambda}_3) F_N | \psi_{abc}^{ijk} \rangle$. To compute the left ground state we can either solve a large-scale linear problem (because we know the ground-state energy E_0), or we use an iterative Arnoldi algorithm for general nonsymmetric eigenvalue problems to compute the ground state of \bar{H}_N . In our experience the latter approach is more stable and requires fewer iterations. The ground-state expectation value of an operator \hat{O} is

$$\langle \hat{O} \rangle \equiv \langle \psi | (1 + \hat{\Lambda}) \bar{O} | \psi \rangle. \quad (7)$$

Here the similarity-transformation $\bar{O} \equiv e^{-\hat{T}} \hat{O} e^{\hat{T}}$ of \hat{O} enters.

The charge radius squared is computed from

$$R_{\text{ch}}^2 = R_p^2 + \langle r_p^2 \rangle + \frac{N}{Z} \langle r_n^2 \rangle + \langle r_{\text{DF}}^2 \rangle + \langle r_{\text{SO}}^2 \rangle. \quad (8)$$

Here, R_p^2 is the mean radius squared of the intrinsic point-proton distribution, and $\langle r_{\text{SO}}^2 \rangle$ is the spin-orbit corrections. These two quantities are actually computed with the coupled-cluster method [4]. The corrections $\langle r_p^2 \rangle = 0.709 \text{ fm}^2$, $\langle r_n^2 \rangle = -0.106 \text{ fm}^2$, and $\langle r_{\text{DF}}^2 \rangle = 3/(4m^2) = 0.033 \text{ fm}^2$ (with m denoting the nucleon mass) are the charge radius squared of the proton (updated according to Refs. [78,79]), the neutron (updated value from Ref. [80]), and the Darwin-Foldy term, respectively.

Results. Our results for the charge radii of magnesium isotopes are shown in Fig. 1. Here, each band reflects model-space uncertainties from using two oscillator frequencies of 12 and 16 MeV. This choice of frequencies is based on Ref. [57] where the convergence of the ^{68}Ni charge radius was studied in detail for similar interactions. The results for the softer interaction with a cutoff of $394 \text{ MeV}c^{-1}$ are shown in red and exhibit less model-space dependence than those for the harder interaction with $450 \text{ MeV}c^{-1}$ shown in blue. Based on these results and our expert judgment we estimate that the uncertainties for the radii, both from the model space and the two interactions are about 2 to 3%, i.e., the full area covered by (and between) both bands. This uncertainty estimate is in line with theory error bars from similar calculations [50,52,57,58]. The experimental uncertainties are smaller than the marker size [38].

Overall, the $\Delta\text{NNLO}_{\text{GO}}$ potentials reproduce the prominent pattern of a minimum radius at the subshell closure $N = 14$, and they agree with data within uncertainties for mass numbers $22 \leq A \leq 30$. The computed radii continue to increase beyond $N = 14$, and they reflect the absence of the $N = 20$ shell closure in magnesium. This is, of course, the beginning of the island of inversion. However, the theory results do not reproduce the very steep increase from $A = 30$ to 32. Thus, they seem to reflect remnants of a shell closure at $N = 20$ that are not seen in the data. Theory predicts increasing charge radii as the dripline is approached. This is consistent with an increase in nuclear deformation as neutrons are added [44]. We also note that theory predicts a marked shell closure at $N = 8$ for neutron-deficient magnesium. This is in contrast to the trend projected in Ref. [38]. The excited 2^+ state in ^{18}Mg at 1.6 MeV is somewhat higher than the 1.2 MeV observed in ^{20}Mg , and the question regarding a subshell closure at $N = 8$ is thus, undecided. It will be interesting to compare the theoretical results with upcoming laser spectroscopy experiments that are at the proposal stage [45].

The plot of isotopic variations in the charge radii, shown in Fig. 3, is interesting. Theory is not accurate regarding most isotopes shifts and overemphasizes shell closures at $N = 14$ and $N = 20$ that are not in the data. This is perhaps a most important result of this study: Whereas state-of-the-art potentials and many-body methods can now describe trends of charge radii, finer details, such as isotope shifts, still escape the computations.

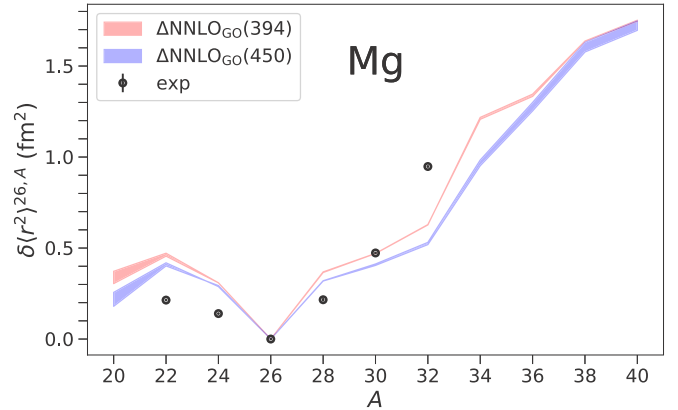


FIG. 3. As in Fig. 1 but for the isotope shift, i.e., the charge radii squared relative to ^{26}Mg . Data taken from Ref. [38].

We show the results for binding energies in Fig. 4. Our calculations yield the dripline at ^{40}Mg with ^{42}Mg being about 1.8 MeV less bound for the $\Delta\text{NNLO}_{\text{GO}}(394)$ potential. However, computational limitations prevented us from including continuum effects, which can easily yield an additional binding energy of the order of 1 MeV [81]. This prevents us from predicting the unknown dripline in magnesium more precisely [82].

Another uncertainty stems from the lack of angular momentum projection. To estimate the corresponding energy correction, we performed a projection after variation within the Hartree-Fock computations. These projections lower the Hartree-Fock energy by about 3–5 MeV, see Fig. 2 for an example. We expect that a projection of the coupled-cluster results would yield slightly less energy gains (because these calculations already include some of the correlations that are associated with a projection). Overall, Fig. 4 shows that the $\Delta\text{NNLO}_{\text{GO}}$ potentials accurately describe nuclear binding energies also for open-shell nuclei.

Binding-energy differences, such as the two-neutron separation energy, is another observable sensitive to shell structure and dripline physics. Figure 5 shows that the overall pattern in the data is accurately reproduced within the uncertainties from the employed interactions and model spaces. Although our radii suggest a subshell closure at $N = 14$, neither theory

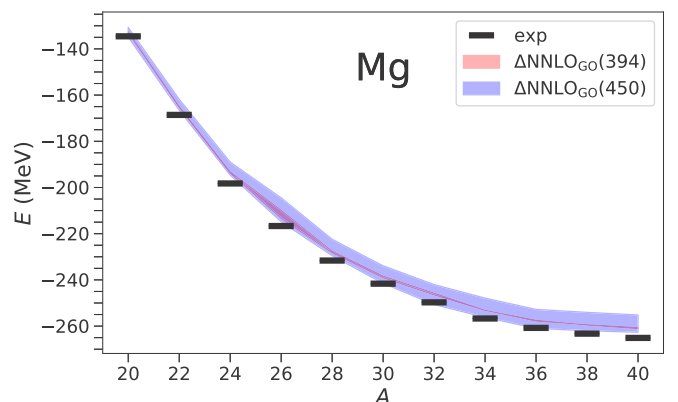


FIG. 4. As in Fig. 1 but for the ground-state energies.

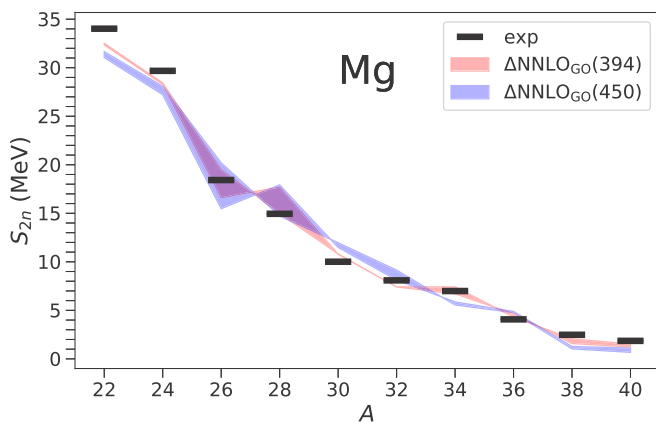


FIG. 5. As in Fig. 1 but for the two-neutron separation energies.

nor data support this closure for the two-neutron separation energies.

We finally turn to neon isotopes. Here, our computations have been less extensive to manage the available computational cycles. We limited the computations of energies to the $\Delta\text{NNLO}_{\text{GO}}(394)$ potentials in a model space of 13 harmonic-oscillator shells at $\hbar\omega = 16$ MeV. For the charge radii we also employed the $\Delta\text{NNLO}_{\text{GO}}(450)$ potential at $\hbar\omega = 12$ MeV. Figure 6 shows that the ground-state energies are close to the data. We estimate theoretical uncertainties to be a bit smaller than for the magnesium isotopes. We also note that about 3–5 MeV of energy gain is expected from a projection of angular momentum (see again Fig. 2). We find the dripline at ^{34}Ne , in agreement with data [83]. Our computations yield that ^{36}Ne is unbound by several MeV, too much to be changed by continuum effects.

The computed two-neutron separation energies, shown in Fig. 7, confirm this picture. Compared to magnesium, it is interesting that the addition of two protons shifts the drip line by about six neutrons. Again we estimate that theoretical uncertainties are a bit smaller than for the magnesium isotopes.

Finally, we show results for charge radii in Fig. 8 using the $\Delta\text{NNLO}_{\text{GO}}(394)$ and $\Delta\text{NNLO}_{\text{GO}}(450)$ potentials. We only

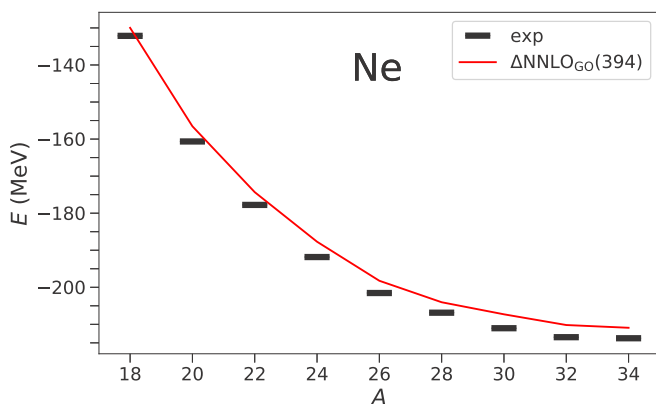


FIG. 6. Ground-state energies for neon isotopes with even mass numbers computed with the potentials $\Delta\text{NNLO}_{\text{GO}}(394)$ shown as a red line. The model spaces consist of 13 oscillator shells. Data [84] are shown as black bars.

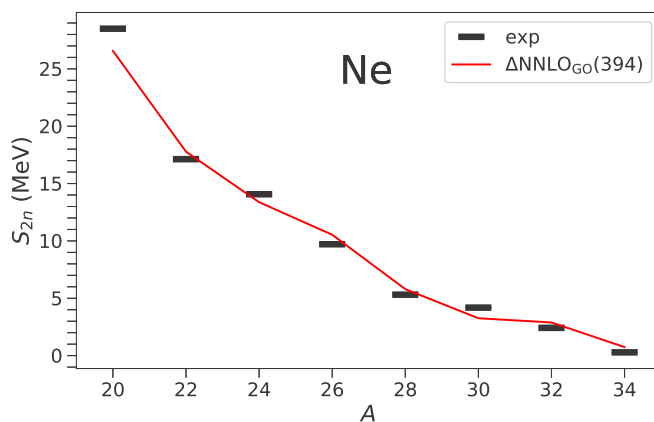


FIG. 7. As in Fig. 6 but for the two-neutron separation energies.

employed one oscillator frequency for each interaction. Thus, the theoretical uncertainties are estimated to be somewhat larger than the area between the two lines (compare with Fig. 1 of the magnesium isotopes). Based on these estimates, theoretical results are not quite accurate below ^{22}Ne , although they qualitatively reproduce the overall trend. The results accurately reflect the known subshell closures at $N = 14$ and $N = 8$. We see no closure at $N = 20$, and it will be interesting to confront this prediction with data.

Conclusion. We computed ground-state energies, two-neutron separation energies, and charge radii for neon and magnesium isotopes. Our computations were based on nucleon-nucleon and three-nucleon potentials from chiral EFT, and we employed coupled-cluster methods that started from an axially symmetric reference state. The computed energies and radii are accurate when taking expected corrections from angular momentum projection into account. Trends in charge radii, and the minimum and neutron number $N = 14$ are qualitatively reproduced. Within our estimated uncertainties of about 2 to 3%, however, quantitative accuracy is not

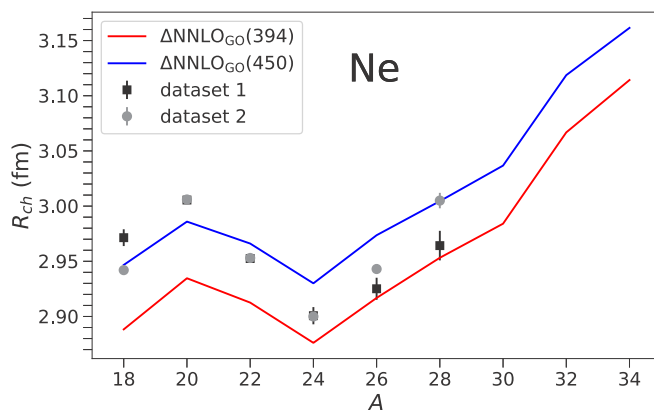


FIG. 8. Charge radii for neon isotopes with even mass numbers computed with the potentials $\Delta\text{NNLO}_{\text{GO}}(394)$ and $\Delta\text{NNLO}_{\text{GO}}(450)$ shown in red and blue, respectively. The model spaces consist of 13 oscillator shells. Data is shown as black squares with statistical and systematic uncertainties [41,42] and as gray circles with statistical uncertainties [43].

achieved for all isotopes, and isotope shifts still challenge theory. Nevertheless, we predict a continuous increase as the neutron dripline is approached, and this is consistent with a considerable nuclear deformation. Proposed experiments will soon confront these predictions.

Acknowledgments. We thank T. Duguet, Z. H. Sun, and A. Tichai for useful discussions. This work was supported by the U.S. Department of Energy, Office of Science, Office

of Nuclear Physics, under Awards No. DE-FG02-96ER40963 and No. DE-SC0018223. Computer time was provided by the Innovative and Novel Computational Impact on Theory and Experiment (INCITE) Program. This research used resources of the Oak Ridge Leadership Computing Facility located at Oak Ridge National Laboratory, which is supported by the Office of Science of the Department of Energy under Contract No. DE-AC05-00OR22725.

-
- [1] I. Tanihata, H. Hamagaki, O. Hashimoto, Y. Shida, N. Yoshikawa, K. Sugimoto, O. Yamakawa, T. Kobayashi, and N. Takahashi, Measurements of Interaction Cross Sections and Nuclear Radii in the Light p -Shell Region, *Phys. Rev. Lett.* **55**, 2676 (1985).
- [2] I. Tanihata, H. Savajols, and R. Kanungo, Recent experimental progress in nuclear halo structure studies, *Prog. Part. Nucl. Phys.* **68**, 215 (2013).
- [3] S. Abrahamyan *et al.*, Measurement of the Neutron Radius of ^{208}Pb Through Parity-Violation in Electron Scattering, *Phys. Rev. Lett.* **108**, 112502 (2012).
- [4] G. Hagen, A. Ekström, C. Forssén, G. R. Jansen, W. Nazarewicz, T. Papenbrock, K. A. Wendt, S. Bacca, N. Barnea, B. Carlsson, C. Drischler, K. Hebeler, M. Hjorth-Jensen, M. Miorelli, G. Orlandini, A. Schwenk, and J. Simonis, Neutron and weak-charge distributions of the ^{48}Ca nucleus, *Nat. Phys.* **12**, 186 (2016).
- [5] M. L. Bissell, T. Crette, K. T. Flanagan, P. Vingerhoets, J. Billowes, K. Blaum, B. Cheal, S. Fritzsche, M. Godefroid, M. Kowalska, J. Krämer, R. Neugart, G. Neyens, W. Nörtershäuser, and D. T. Jordanov, Cu charge radii reveal a weak sub-shell effect at $N = 40$, *Phys. Rev. C* **93**, 064318 (2016).
- [6] R. F. Garcia Ruiz, M. L. Bissell, K. Blaum, A. Ekström, N. Frömmgen, G. Hagen, M. Hammen, K. Hebeler, J. D. Holt, G. R. Jansen, M. Kowalska, K. Kreim, W. Nazarewicz, R. Neugart, G. Neyens, W. Nörtershäuser, T. Papenbrock, J. Papuga, A. Schwenk, J. Simonis, K. A. Wendt, and D. T. Jordanov, Unexpectedly large charge radii of neutron-rich calcium isotopes, *Nat. Phys.* **12**, 594 (2016).
- [7] A. J. Miller, K. Minamisono, A. Klose, D. Garand, C. Kujawa, J. D. Lantis, Y. Liu, B. Maaß, P. F. Mantica, W. Nazarewicz, W. Nörtershäuser, S. V. Pineda, P. G. Reinhard, D. M. Rossi, F. Sommer, C. Sumithrarachchi, A. Teigelhöfer, and J. Watkins, Proton superfluidity and charge radii in proton-rich calcium isotopes, *Nat. Phys.* **15**, 432 (2019).
- [8] R. P. de Groote, J. Billowes, C. L. Binnersley, M. L. Bissell, T. E. Cocolios, T. Day Goodacre, G. J. Farooq-Smith, D. V. Fedorov, K. T. Flanagan, S. Franchoo, R. F. Garcia Ruiz, W. Gins, J. D. Holt, Á. Koszorús, K. M. Lynch, T. Miyagi, W. Nazarewicz, G. Neyens, P. G. Reinhard, S. Rothe, H. H. Stroke, A. R. Vernon, K. D. A. Wendt, S. G. Wilkins, Z. Y. Xu, and X. F. Yang, Measurement and microscopic description of odd-even staggering of charge radii of exotic copper isotopes, *Nat. Phys.* **16**, 620 (2020).
- [9] Steven C. Pieper and R. B. Wiringa, Quantum Monte Carlo calculations of light nuclei, *Annu. Rev. Nucl. Part. Sci.* **51**, 53 (2001).
- [10] P. Navrátil, S. Quaglioni, I. Stetcu, and B. R. Barrett, Recent developments in no-core shell-model calculations, *J. Phys. G: Nucl. Part. Phys.* **36**, 083101 (2009).
- [11] B. R. Barrett, P. Navrátil, and J. P. Vary, *Ab initio* no core shell model, *Prog. Part. Nucl. Phys.* **69**, 131 (2013).
- [12] J. Carlson, S. Gandolfi, F. Pederiva, S. C. Pieper, R. Schiavilla, K. E. Schmidt, and R. B. Wiringa, Quantum Monte Carlo methods for nuclear physics, *Rev. Mod. Phys.* **87**, 1067 (2015).
- [13] U. van Kolck, Few-nucleon forces from chiral Lagrangians, *Phys. Rev. C* **49**, 2932 (1994).
- [14] D. R. Entem and R. Machleidt, Accurate charge-dependent nucleon-nucleon potential at fourth order of chiral perturbation theory, *Phys. Rev. C* **68**, 041001(R) (2003).
- [15] E. Epelbaum, H.-W. Hammer, and Ulf-G. Meißner, Modern theory of nuclear forces, *Rev. Mod. Phys.* **81**, 1773 (2009).
- [16] R. Machleidt and D.R. Entem, Chiral effective field theory and nuclear forces, *Phys. Rep.* **503**, 1 (2011).
- [17] K. Hebeler, S. K. Bogner, R. J. Furnstahl, A. Nogga, and A. Schwenk, Improved nuclear matter calculations from chiral low-momentum interactions, *Phys. Rev. C* **83**, 031301(R) (2011).
- [18] A. Ekström, G. R. Jansen, K. A. Wendt, G. Hagen, T. Papenbrock, B. D. Carlsson, C. Forssén, M. Hjorth-Jensen, P. Navrátil, and W. Nazarewicz, Accurate nuclear radii and binding energies from a chiral interaction, *Phys. Rev. C* **91**, 051301(R) (2015).
- [19] S. K. Bogner, T. T. S. Kuo, and A. Schwenk, Model-independent low momentum nucleon interaction from phase shift equivalence, *Phys. Rep.* **386**, 1 (2003).
- [20] S. K. Bogner, R. J. Furnstahl, and R. J. Perry, Similarity renormalization group for nucleon-nucleon interactions, *Phys. Rev. C* **75**, 061001(R) (2007).
- [21] S. K. Bogner, R. J. Furnstahl, and A. Schwenk, From low-momentum interactions to nuclear structure, *Prog. Part. Nucl. Phys.* **65**, 94 (2010).
- [22] B. Mihaila and J. H. Heisenberg, Microscopic Calculation of the Inclusive Electron Scattering Structure Function in ^{16}O , *Phys. Rev. Lett.* **84**, 1403 (2000).
- [23] D. J. Dean and M. Hjorth-Jensen, Coupled-cluster approach to nuclear physics, *Phys. Rev. C* **69**, 054320 (2004).
- [24] G. Hagen, T. Papenbrock, M. Hjorth-Jensen, and D. J. Dean, Coupled-cluster computations of atomic nuclei, *Rep. Prog. Phys.* **77**, 096302 (2014).
- [25] K. Tsukiyama, S. K. Bogner, and A. Schwenk, In-Medium Similarity Renormalization Group For Nuclei, *Phys. Rev. Lett.* **106**, 222502 (2011).
- [26] H. Hergert, S. K. Bogner, T. D. Morris, A. Schwenk, and K. Tsukiyama, The in-medium similarity renormalization group: A novel *ab initio* method for nuclei, *Phys. Rep.* **621**, 165 (2016).
- [27] D. Lee, Lattice simulations for few- and many-body systems, *Prog. Part. Nucl. Phys.* **63**, 117 (2009).

- [28] T. A. Lähde, E. Epelbaum, H. Krebs, D. Lee, U.-G. Meißner, and G. Rupak, Lattice effective field theory for medium-mass nuclei, *Phys. Lett. B* **732**, 110 (2014).
- [29] T. Dytrych, K. D. Launey, J. P. Draayer, D. J. Rowe, J. L. Wood, G. Rosensteel, C. Bahri, D. Langr, and R. B. Baker, Physics of Nuclei: Key Role of an Emergent Symmetry, *Phys. Rev. Lett.* **124**, 042501 (2020).
- [30] W. H. Dickhoff and C. Barbieri, Self-consistent Green's function method for nuclei and nuclear matter, *Prog. Part. Nucl. Phys.* **52**, 377 (2004).
- [31] V. Somà, C. Barbieri, and T. Duguet, *Ab initio* Gorkov-Green's function calculations of open-shell nuclei, *Phys. Rev. C* **87**, 011303(R) (2013).
- [32] T. D. Morris, J. Simonis, S. R. Stroberg, C. Stumpf, G. Hagen, J. D. Holt, G. R. Jansen, T. Papenbrock, R. Roth, and A. Schwenk, Structure of the Lightest Tin Isotopes, *Phys. Rev. Lett.* **120**, 152503 (2018).
- [33] P. Gysbers, G. Hagen, J. D. Holt, G. R. Jansen, T. D. Morris, P. Navrátil, T. Papenbrock, S. Quaglioni, A. Schwenk, S. R. Stroberg, and K. A. Wendt, Discrepancy between experimental and theoretical β -decay rates resolved from first principles, *Nat. Phys.* **15**, 428 (2019).
- [34] J. D. Holt, S. R. Stroberg, A. Schwenk, and J. Simonis, *Ab initio* limits of atomic nuclei, [arXiv:1905.10475](https://arxiv.org/abs/1905.10475).
- [35] M. Bender, P.-H. Heenen, and P.-G. Reinhard, Self-consistent mean-field models for nuclear structure, *Rev. Mod. Phys.* **75**, 121 (2003).
- [36] T. Nikšić, D. Vretenar, and P. Ring, Relativistic nuclear energy density functionals: Mean-field and beyond, *Prog. Part. Nucl. Phys.* **66**, 519 (2011).
- [37] J. Erler, N. Birge, M. Kortelainen, W. Nazarewicz, E. Olsen, A. M. Perhac, and M. Stoitsov, The limits of the nuclear landscape, *Nature (London)* **486**, 509 (2012).
- [38] D. T. Yordanov, M. L. Bissell, K. Blaum, M. De Rydt, Ch. Geppert, M. Kowalska, J. Krämer, K. Kreim, A. Krieger, P. Lievens, T. Neff, R. Neugart, G. Neyens, W. Nörtershäuser, R. Sánchez, and P. Vingerhoets, Nuclear Charge Radii of $^{21-32}\text{Mg}$, *Phys. Rev. Lett.* **108**, 042504 (2012).
- [39] A. Poves and J. Retamosa, The onset of deformation at the $N = 20$ neutron shell closure far from stability, *Phys. Lett. B* **184**, 311 (1987).
- [40] E. K. Warburton, J. A. Becker, and B. A. Brown, Mass systematics for $A = 29-44$ nuclei: The deformed $A \sim 32$ region, *Phys. Rev. C* **41**, 1147 (1990).
- [41] K. Marinova, W. Geithner, M. Kowalska, K. Blaum, S. Kappertz, M. Keim, S. Kloos, G. Kotrotsios, P. Lievens, R. Neugart, H. Simon, and S. Wilbert, Charge radii of neon isotopes across the sd neutron shell, *Phys. Rev. C* **84**, 034313 (2011).
- [42] I. Angeli and K. P. Marinova, Table of experimental nuclear ground state charge radii: An update, *At. Data Nucl. Data Tables* **99**, 69 (2013).
- [43] B. Ohayon, H. Rahangdale, A. J. Geddes, J. C. Berengut, and G. Ron, Isotope shifts in $^{20,22}\text{Ne}$: Precision measurements and global analysis in the framework of intermediate coupling, *Phys. Rev. A* **99**, 042503 (2019).
- [44] H. L. Crawford, P. Fallon, A. O. Macchiavelli, P. Doornenbal, N. Aoi, F. Browne, C. M. Campbell, S. Chen, R. M. Clark, M. L. Cortés, M. Cromaz, E. Ideguchi, M. D. Jones, R. Kanungo, M. MacCormick, S. Momiyama, I. Murray, M. Niikura, S. Paschalis, M. Petri, H. Sakurai, M. Salathe, P. Schrock, D. Steppenbeck, S. Takeuchi, Y. K. Tanaka, R. Taniuchi, H. Wang, and K. Wimmer, First Spectroscopy of the Near Drip-Line Nucleus ^{40}Mg , *Phys. Rev. Lett.* **122**, 052501 (2019).
- [45] M. Vilén, S. Malbrunot-Ettenauer, P. Fischer, H. Heylen, V. Lagaki, S. Lechner, F. M. Maier, W. Nörtershäuser, P. Plattner, S. Sels, L. Schweikhard, and F. Wienholtz, MIRACLS at ISOLDE: The Charge Radii of Exotic Magnesium Isotopes, (2020).
- [46] A. Ekström, G. Baardsen, C. Forssén, G. Hagen, M. Hjorth-Jensen, G. R. Jansen, R. Machleidt, W. Nazarewicz, T. Papenbrock, J. Sarich, and S. M. Wild, Optimized Chiral Nucleon-Nucleon Interaction at Next-To-Next-To-Leading Order, *Phys. Rev. Lett.* **110**, 192502 (2013).
- [47] D. R. Entem, N. Kaiser, R. Machleidt, and Y. Nosyk, Peripheral nucleon-nucleon scattering at fifth order of chiral perturbation theory, *Phys. Rev. C* **91**, 014002 (2015).
- [48] E. Epelbaum, H. Krebs, and U.-G. Meißner, Precision Nucleon-Nucleon Potential at Fifth Order in the Chiral Expansion, *Phys. Rev. Lett.* **115**, 122301 (2015).
- [49] T. Hüther, K. Vobig, K. Hebeler, R. Machleidt, and R. Roth, Family of Chiral Two- plus Three-Nucleon Interactions for Accurate Nuclear Structure Studies, *Phys. Lett. B*, **808**, 135651 (2020).
- [50] V. Somà, P. Navrátil, F. Raimondi, C. Barbieri, and T. Duguet, Novel chiral Hamiltonian and observables in light and medium-mass nuclei, *Phys. Rev. C* **101**, 014318 (2020).
- [51] C. G. Payne, S. Bacca, G. Hagen, W. G. Jiang, and T. Papenbrock, Coherent elastic neutrino-nucleus scattering on ^{40}Ar from first principles, *Phys. Rev. C* **100**, 061304(R) (2019).
- [52] S. Bagchi, R. Kanungo, Y. K. Tanaka, H. Geissel, P. Doornenbal, W. Horiuchi, G. Hagen, T. Suzuki, N. Tsunoda, D. S. Ahn, H. Baba, K. Behr, F. Browne, S. Chen, M. L. Cortés, A. Estradé, N. Fukuda, M. Holl, K. Itahashi, N. Iwasa, G. R. Jansen, W. G. Jiang, S. Kaur, A. O. Macchiavelli, S. Y. Matsumoto, S. Momiyama, I. Murray, T. Nakamura, S. J. Novario, H. J. Ong, T. Otsuka, T. Papenbrock, S. Paschalis, A. Prochazka, C. Scheidenberger, P. Schrock, Y. Shimizu, D. Steppenbeck, H. Sakurai, D. Suzuki, H. Suzuki, M. Takechi, H. Takeda, S. Takeuchi, R. Taniuchi, K. Wimmer, and K. Yoshida, Two-Neutron Halo is Unveiled in ^{29}F , *Phys. Rev. Lett.* **124**, 222504 (2020).
- [53] W. G. Jiang, A. Ekström, C. Forssén, G. Hagen, G. R. Jansen, and T. Papenbrock, Accurate bulk properties of nuclei from $A = 2$ to ∞ from potentials with Δ isobars, *Phys. Rev. C* **102**, 054301 (2020).
- [54] K. Hebeler, H. Krebs, E. Epelbaum, J. Golak, and R. Skibiński, Efficient calculation of chiral three-nucleon forces up to N^3LO for *ab initio* studies, *Phys. Rev. C* **91**, 044001 (2015).
- [55] J. Simonis, S. R. Stroberg, K. Hebeler, J. D. Holt, and A. Schwenk, Saturation with chiral interactions and consequences for finite nuclei, *Phys. Rev. C* **96**, 014303 (2017).
- [56] G. Hagen, G. R. Jansen, and T. Papenbrock, Structure of ^{78}Ni from First-Principles Computations, *Phys. Rev. Lett.* **117**, 172501 (2016).
- [57] S. Kaufmann, J. Simonis, S. Bacca, J. Billowes, M. L. Bissell, K. Blaum, B. Cheal, R. F. Garcia Ruiz, W. Gins, C. Gorges, G. Hagen, H. Heylen, A. Kanellakopoulos, S. Malbrunot-Ettenauer, M. Miorelli, R. Neugart, G. Neyens, W. Nörtershäuser, R. Sánchez, S. Sailer, A. Schwenk, T. Ratajczyk,

- L. V. Rodríguez, L. Wehner, C. Wraith, L. Xie, Z. Y. Xu, X. F. Yang, and D. T. Jordanov, Charge Radius of the Short-Lived ^{68}Ni and Correlation with the Dipole Polarizability, *Phys. Rev. Lett.* **124**, 132502 (2020).
- [58] V. Somà, C. Barbieri, T. Duguet, and P. Navrátil, Moving away from singly-magic nuclei with Gorkov Green's function theory, [arXiv:2009.01829](https://arxiv.org/abs/2009.01829).
- [59] A. Tichai, J. Müller, K. Vobig, and R. Roth, Natural orbitals for *ab initio* no-core shell model calculations, *Phys. Rev. C* **99**, 034321 (2019).
- [60] G. Hagen, T. Papenbrock, D. J. Dean, and M. Hjorth-Jensen, *Ab initio* coupled-cluster approach to nuclear structure with modern nucleon-nucleon interactions, *Phys. Rev. C* **82**, 034330 (2010).
- [61] C. Yannouleas and U. Landman, Spontaneous Symmetry Breaking in Single and Molecular Quantum Dots, *Phys. Rev. Lett.* **82**, 5325 (1999).
- [62] T. Duguet, Symmetry broken and restored coupled-cluster theory: I. Rotational symmetry and angular momentum, *J. Phys. G: Nucl. Part. Phys.* **42**, 025107 (2015).
- [63] Y. Qiu, T. M. Henderson, J. Zhao, and G. E. Scuseria, Projected coupled cluster theory, *J. Chem. Phys.* **147**, 064111 (2017).
- [64] Y. Qiu, T. M. Henderson, J. Zhao, and G. E. Scuseria, Projected coupled cluster theory: Optimization of cluster amplitudes in the presence of symmetry projection, *J. Chem. Phys.* **149**, 164108 (2018).
- [65] T. Tsuchimochi and S. L. Ten-no, Orbital-invariant spin-extended approximate coupled-cluster for multi-reference systems, *J. Chem. Phys.* **149**, 044109 (2018).
- [66] P. Möller, R. Bengtsson, B. G. Carlsson, P. Olivius, and T. Ichikawa, Global Calculations of Ground-State Axial Shape Asymmetry of Nuclei, *Phys. Rev. Lett.* **97**, 162502 (2006).
- [67] I. Shavitt and R. J. Bartlett, *Many-body Methods in Chemistry and Physics* (Cambridge University Press, Cambridge, UK, 2009).
- [68] J. Ripoché, A. Tichai, and T. Duguet, Normal-ordered k -body approximation in particle-number-breaking theories, *Eur. Phys. J. A* **56**, 40 (2020).
- [69] F. Coester, Bound states of a many-particle system, *Nucl. Phys.* **7**, 421 (1958).
- [70] H. Kümmel, K. H. Lührmann, and J. G. Zabolitzky, Many-fermion theory in expS- (or coupled cluster) form, *Phys. Rep.* **36**, 1 (1978).
- [71] R. F. Bishop, An overview of coupled cluster theory and its applications in physics, *Theor. Chim. Acta* **80**, 95 (1991).
- [72] R. J. Bartlett and M. Musiał, Coupled-cluster theory in quantum chemistry, *Rev. Mod. Phys.* **79**, 291 (2007).
- [73] S. Binder, P. Piecuch, A. Calci, J. Langhammer, P. Navrátil, and R. Roth, Extension of coupled-cluster theory with a noniterative treatment of connected triply excited clusters to three-body hamiltonians, *Phys. Rev. C* **88**, 054319 (2013).
- [74] Y. S. Lee, S. A. Kucharski, and R. J. Bartlett, A coupled cluster approach with triple excitations, *J. Chem. Phys.* **81**, 5906 (1984).
- [75] J. D. Watts and R. J. Bartlett, Economical triple excitation equation-of-motion coupled-cluster methods for excitation energies, *Chem. Phys. Lett.* **233**, 81 (1995).
- [76] J. F. Stanton and R. J. Bartlett, The equation of motion coupled-cluster method. a systematic biorthogonal approach to molecular excitation energies, transition probabilities, and excited state properties, *J. Chem. Phys.* **98**, 7029 (1993).
- [77] M. Miorelli, S. Bacca, G. Hagen, and T. Papenbrock, Computing the dipole polarizability of ^{48}Ca with increased precision, *Phys. Rev. C* **98**, 014324 (2018).
- [78] R. Pohl, A. Antognini, F. Nez, F. D. Amaro, F. Biraben, J. M. R. Cardoso, D. S. Covita, A. Dax, S. Dhawan, L. M. P. Fernandes, A. Giesen, T. Graf, T. W. Hänsch, P. Indelicato, L. Julien, C.-Y. Kao, P. Knowles, E.-O. Le Bigot, Y.-W. Liu, José A. M. Lopes, L. Ludhova, C. M. B. Monteiro, F. Mulhauser, T. Nebel, P. Rabinowitz, J. M. F. Dos Santos, L. A. Schaller, K. Schuhmann, C. Schwob, D. Taqqu, Jo. F. C. A. Veloso, and F. Kottmann, The size of the proton, *Nature (London)* **466**, 213 (2010).
- [79] W. Xiong, A. Gasparian, H. Gao, D. Dutta, M. Khandaker, N. Liyanage, E. Pasyuk, C. Peng, X. Bai, L. Ye, K. Gnanvo, C. Gu, M. Levillain, X. Yan, D. W. Higinbotham, M. Meziane, Z. Ye, K. Adhikari, B. Aljawrneh, H. Bhatt, D. Bhetuwal, J. Brock, V. Burkert, C. Carlin, A. Deur, D. Di, J. Dunne, P. Ekanayaka, L. El-Fassi, B. Emmich, L. Gan, O. Glamazdin, M. L. Kabir, A. Karki, C. Keith, S. Kowalski, V. Lagerquist, I. Larin, T. Liu, A. Liyanage, J. Maxwell, D. Meekins, S. J. Nazeer, V. Nelyubin, H. Nguyen, R. Pedroni, C. Perdrisat, J. Pierce, V. Punjabi, M. Shabestari, A. Shahinyan, R. Silwal, S. Stepanyan, A. Subedi, V. V. Tarasov, N. Ton, Y. Zhang, and Z. W. Zhao, A small proton charge radius from an electron-proton scattering experiment, *Nature (London)* **575**, 147 (2019).
- [80] A. A. Filin, V. Baru, E. Epelbaum, H. Krebs, D. Möller, and P. Reinert, Extraction of the Neutron Charge Radius from a Precision Calculation of the Deuteron Structure Radius, *Phys. Rev. Lett.* **124**, 082501 (2020).
- [81] G. Hagen, M. Hjorth-Jensen, G. R. Jansen, and T. Papenbrock, Emergent properties of nuclei from *ab initio* coupled-cluster calculations, *Phys. Scr.* **91**, 063006 (2016).
- [82] T. Baumann, A. M. Amthor, D. Bazin, B. A. Brown, C. M. Folden, A. Gade, T. N. Ginter, M. Hausmann, M. Matos, D. J. Morrissey, M. Portillo, A. Schiller, B. M. Sherrill, A. Stolz, O. B. Tarasov, and M. Thoennessen, Discovery of ^{40}Mg and ^{42}Al suggests neutron drip-line slant towards heavier isotopes, *Nature (London)* **449**, 1022 (2007).
- [83] D. S. Ahn, N. Fukuda, H. Geissel, N. Inabe, N. Iwasa, T. Kubo, K. Kusaka, D. J. Morrissey, D. Murai, T. Nakamura, M. Ohtake, H. Otsu, H. Sato, B. M. Sherrill, Y. Shimizu, H. Suzuki, H. Takeda, O. B. Tarasov, H. Ueno, Y. Yanagisawa, and K. Yoshida, Location of the Neutron Dripline at Fluorine and Neon, *Phys. Rev. Lett.* **123**, 212501 (2019).
- [84] M. Wang, G. Audi, A.H. Wapstra, F.G. Kondev, M. MacCormick, X. Xu, and B. Pfeiffer, The AME2012 atomic mass evaluation, *Chin. Phys. C* **36**, 1603 (2012).